



This is a repository copy of *Ultrafast Dynamics of the Photo-Excited Hemes b and cn in the Cytochrome b6f Complex*.

White Rose Research Online URL for this paper:

<https://eprints.whiterose.ac.uk/110209/>

Version: Accepted Version

Article:

Agarwal, R. and Chauvet, A.A.P. (2017) Ultrafast Dynamics of the Photo-Excited Hemes b and cn in the Cytochrome b6f Complex. *Physical Chemistry Chemical Physics*, 2017 (4). pp. 3287-3296. ISSN 1463-9076

<https://doi.org/10.1039/C6CP08077D>

Reuse

Items deposited in White Rose Research Online are protected by copyright, with all rights reserved unless indicated otherwise. They may be downloaded and/or printed for private study, or other acts as permitted by national copyright laws. The publisher or other rights holders may allow further reproduction and re-use of the full text version. This is indicated by the licence information on the White Rose Research Online record for the item.

Takedown

If you consider content in White Rose Research Online to be in breach of UK law, please notify us by emailing eprints@whiterose.ac.uk including the URL of the record and the reason for the withdrawal request.



eprints@whiterose.ac.uk
<https://eprints.whiterose.ac.uk/>

Ultrafast Dynamics of the Photo-Excited Hemes *b* and *c_n* in the Cytochrome *b₆f* Complex.

Received 00th January 20xx,
Accepted 00th January 20xx

Rachna Agarwal,^{a, b} Adrien A. P. Chauvet^{c*†}

DOI: 10.1039/x0xx00000x

www.rsc.org/

The dynamics of the heme *b* and *c_n* within the cytochrome *b₆f* complex are investigated by means of ultrafast broad-band transient absorption spectroscopy. On one hand, the data reveals that, subsequent to visible light excitation, part of the *b* hemes undergo a pulse limited photo-oxidation, with the liberated electron supposedly being admitted in one of the adjacent aromatic amino acid. The photo-oxidation is followed by a charge recombination in about 8.2 ps. Subsequent to the charge recombination, the heme is promoted to an vibrationally excited ground state that relaxes in about 4.6 ps. On the other hand, the heme *c_n* undergoes an ultrafast ground state recovery in about 140 fs. Interestingly, the data also shows that, contrarily to previous beliefs, Chl *a* is involved in the hemes photochemistry. Indeed, subsequently to the hemes excitation, the Chl *a* bleaches and recovers its ground state in 90 fs and 650 fs, respectively. The Chl *a* bleaching allegedly corresponds to the formation of a short lived Chl *a* anion. Beyond the previously suggested structural role, this study gives unique evidences that Chl *a* is directly involved in the photochemistry of the hemes.

Introduction

The role of the cytochrome (cyt) *b₆f* complex is central to the oxygenic photosynthetic apparatus of all plants, green algae, and cyanobacteria as it participates in generating the proton electrochemical potential gradient across the thylakoid membrane.¹ The physiological functions of the cyt *b₆f* complex are therefore similar to the homologous cyt *bc₁* complex in mitochondria and photosynthetic bacteria.^{2, 3} The cyt *b₆f* complex however differs from cyt *bc₁* in terms of its structure as it contains an additional molecule of β -carotene (Car), chlorophyll *a* (Chl *a*) and an additional *c*-type heme, called *c_n*, on the electrochemically negative side of the complex in each monomer (Figure 1).¹ In contrast to the 6-coordinated (6-c) low-spin iron centers of the hemes *b_p* and *b_n*, and their bi-histidine (His) axial ligation, the heme *c_n* distinguishes itself by its 5-c high-spin iron center whose only axial ligand is a H₂O or OH⁻ molecule.⁴ There are no previous ultrafast studies of the hemes *b_p*, *b_n* nor *c_n* dynamics within the cyt *b₆f* complex. The high sensitivity of the cyt *b₆f* sample to molecular oxygen⁵ and the limited quantity of spectroscopy-grade sample available are certainly the main reasons behind the absence of such studies.

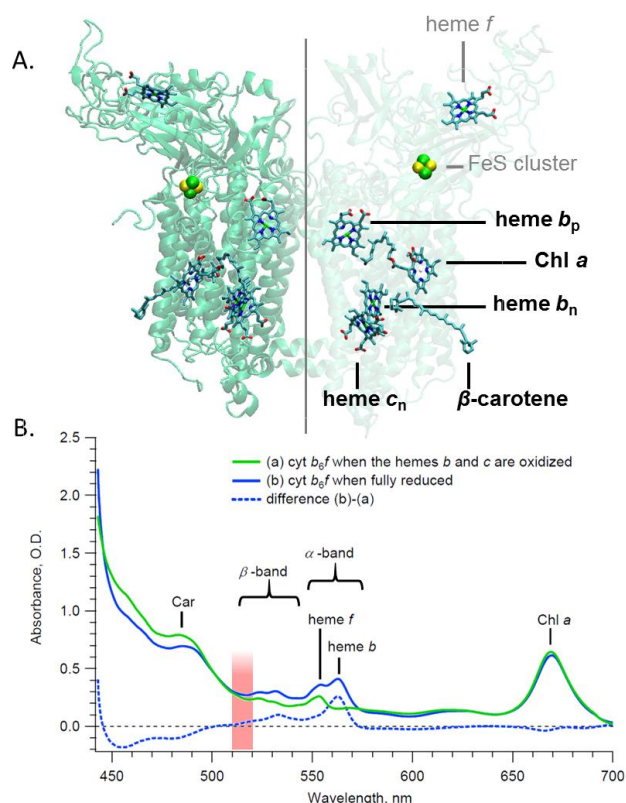


Figure 1: (A) Prosthetic groups of the cyt *b₆f* complex, from the crystallographic PDB file 2E74.⁶ (B) Absorbance spectra of the cyt *b₆f* complex before (green) and after (blue) addition of dithionite, which effectively reduces all hemes. The amplitude scale is adjusted so that the static spectrum is zero after 720 nm. The difference spectrum is shown (dashed blue). The red-shaded area corresponds to the 515 nm laser excitation.

^a Department of Biological Sciences, Purdue University, West Lafayette, Indiana 47907, United States.

^b Molecular Biology Division, Bhabha Atomic Research Centre, Mumbai 400 085, India.

^c Ecole Polytechnique Fédérale de Lausanne (EPFL), Laboratoire de Spectroscopie Ultrarapide (LSU), ISIC, Faculté des Sciences de Base and Lausanne Centre for Ultrafast Science (LACUS), Station 6, 1015 Lausanne, Switzerland.

* Corresponding Author: a.chauvet@sheffield.ac.uk

† Present Addresses: The University of Sheffield, Department of Chemistry, Dainton Building, Brook Hill, Sheffield S3 7HF, United Kingdom.

The present work is a direct application of the recent technological development in microfluidic systems⁷ and miniaturisation of anaerobic chambers⁵ that were specifically designed for this study. In line with the previous investigation of the cyt *b_{6f}* heme *f* dynamics,⁸ the aim of the present study is to resolve the ultrafast response of the photo-excited hemes *b_p*, *b_n* and *c_n* and their interaction with the near-by Chl *a* and Car molecules.

The relevance of ultrafast investigation of heme-embedded proteins is to access the early time mechanisms and local structural and electronic modifications that confer the protein complex its overall functions. The ultrafast behaviours, and more specifically, the relaxation of photo-excited hemes, have indeed been the object of an intense study since the late 1980s.^{9, 10} For example, the ferrous *b*-hemes in the homologous cyt *bc₁* complex have been found to undergo efficient photo-dissociation and -oxidation within femtoseconds after visible light excitation.¹¹ While photo-dissociation seems to be a rather standard feature in heme-embedded proteins,^{9, 12} the initiation of a charge separated state is intriguing within a complex that is directly involved in cross-membrane proton-coupled-electron transfer.¹ The cyt *b_{6f}* complex, as part of the photosynthetic pathway, is naturally exposed to sun light. It is consequently of great interest to investigate its excited state dynamics and to compare to the homologous cyt *bc₁* complex present in animals. The present study shows that, beside the purely electronic and vibrational relaxation of the heme *b* and *c_n*, part of the *b*-hemes in cyt *b_{6f}* undergoes photo-oxidation. The implication of photo-oxidation as a recurrent relaxation mechanism in heme proteins is briefly discussed.

Furthermore, the proximity of the embedded hemes with the Car and Chl *a* chromophores suggests that both Car and Chl *a* are potentially involved in the deactivation process of the photo-excited hemes, as it is commonly the case in photosynthetic organisms.¹³ The presence of Car and Chl *a* and their physiological significance has been extensively discussed.¹⁴ For a long time, it has been proposed that both Car and Chl *a* are simple evolutionary relics.¹⁵ However, the ability of Chl *a* to generate singlet oxygen¹⁶ and its harmful repercussions on the protein, as discussed by Savikhin et al.,^{17, 18} has kept the mystery alive. The potential perniciousness of photo-excited Chl *a* implies that, if devoid of clear physiological functions, it is safer to remove it rather than providing extra protection mechanisms such as the Car molecule. It has so far been suggested that both the carotenoid and chlorophyll have purely structural functions: the β -carotene protruding 11 Å from the complex could serve as a latch to the Photosystem I Reaction Center,¹⁹ and the chlorophyll through its phytyl chain could serve as a gate for transfer of plastoquinol/quinone.²⁰ The present study adds a new photo-chemical dimension to the current understanding of the protein by showing that, within the cyt *b_{6f}* complex, Chl *a* participates in the ground state recovery of the hemes.

Material and Methods

Purification of Cytochrome *b_{6f}* Complex. Active dimeric cytochrome *b_{6f}* complex was isolated from leaves of *Spinacea* as previously described.²¹ Briefly ~400 g of baby spinach leaves in early growth phase were macerated in grinding buffer (Tris-HCl, 50 mM, pH 7.5; NaCl, 100 mM; sucrose 200 mM; protease inhibitors) at 4°C and the homogenate was filtered and centrifuged at 10,000 x g for 30 min (4°C) to obtain chloroplasts. The chloroplasts were osmotically shocked (10 mM Tris-HCl, pH 8.0 at 4°C, and protease inhibitors) and washed with 2 M NaBr (in Tris 10 mM, pH 8.0 at 4°C), and centrifuged at 10,000 x g for 30 min (4°C). The resulting pellet was resuspended in TNE-sucrose buffer (Tris-HCl 30 mM, pH 7.5, NaCl 50 mM, EDTA 1 mM, 10% sucrose and protease inhibitors). Detergent extraction was performed with 0.9% β -octyl glucoside and 0.1% sodium cholate at a Chl *a* concentration of 2 mg/ml for 25 minutes at room temperature. Insoluble material was removed by ultracentrifugation at 300,000 x g for 45 min at 4°C. The supernatant was further enriched in cyt *b_{6f}* by precipitation of contaminating proteins with 35% ammonium sulfate and removal by ultra-centrifugation at 300,000 x g for 20 minutes at 4°C. Cyt *b_{6f}* in the supernatant was purified by propyl-agarose hydrophobic column chromatography with 0.05% undecyl maltoside (UDM). The *b_{6f}* monomer and dimer were separated on a 10-32% sucrose density gradient centrifugation.²¹ Dimeric cyt *b_{6f}* complex was concentrated and the buffer exchanged to TNE-UDM (0.05%). The subunit composition of the *b_{6f}* preparation was assessed by SDS-PAGE, CN-PAGE, and redox difference spectra using standard procedures. All assays were performed in 30 mM Tris-HCl (pH 7.5), 50 mM NaCl, 0.2 mM EDTA, and 0.04 % UDM. The electron transport activity of the dimeric complex, 150 -200 electrons/cyt *f* - sec, was assessed using decyl-plastoquinol as electron donor and *Chlamydomonas* plastocyanin as electron acceptor.²²

Sample handling for kinetic measurements. The sample was housed in a bespoke microfluidic flow-cell.⁷ In brief, the flow-through cell requires a minimal sample volume of only ~250 μ L that flows into a fixed square quartz silica capillary of 0.5-mm path-length and 0.25-mm thick window. The flow is generated by a Turbisc (friction-based) micro-pump from the Swiss Center for Electronics and Microtechnology (CSEM)²³ and bubbles are removed from the circuit via a decantation chamber. The generated flow of ~0.1 mL/s is sufficient to refresh the sample for each laser shot at 1 kHz repetition rate. The absorbance spectrum, and consequently the oxidation state of the hemes as well as the possible degradation of the complexes was directly monitored via the probe beam. The absorbance spectra shown correspond to an average of all "un-excited" spectra recorded over the different scans for a particular sample condition. The cyt *b_{6f}* complex was studied under controlled atmosphere by means of a miniature anaerobic chamber (1L) specifically designed for the requirement of the experiment.⁵ Under a controlled atmosphere, the reduced state of the hemes was stable over the course of the entire study.

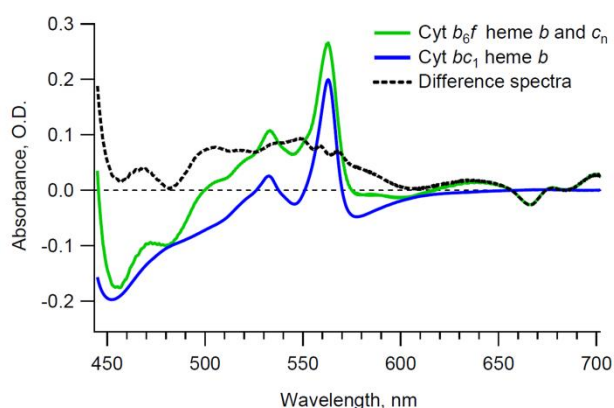


Figure 2: Reduced-minus-oxidized spectrum of the hemes b and c_n from *cyt b_{6f}* (green) superimposed with the reduced-minus-oxidized spectrum of the heme b from *cyt bc₁* (blue),¹¹ red-shifted by 1.2 nm in order for both α -bands to coincide. The difference spectrum is shown in black (dashed).

Transient absorption spectroscopy. The 800-nm output of a 1 kHz regenerative amplifier is used to pump a home-made visible non-colinear optical parametric amplifier (NOPA, see ref.²⁴ for a detailed description) producing the ~ 50 fs, 515-nm pump pulses with a full-width-half-maximum of 11 nm. The excitation is tuned at 515 nm in order to avoid any scattered light from the pump in the region of interest. A small fraction of the regenerative amplifier output is focused onto a 5-mm thick CaF_2 crystal to provide an extended visible probe. The pump and probe pulses are focused into spots of ~ 100 and ~ 50 μm in diameter, respectively, at the sample position by means of reflective optics in order to avoid degradation of the instrument response function. The resulting pump-probe cross-correlation signal is about 150 fs. The polarization of the pump and probe beam were set parallel in order to enhance the otherwise weak Chl a stimulated emission (SE).¹⁵ The SE signal probed with parallel polarization is expected to be about twice as large in amplitude than that monitored with magic angle.¹⁵ Differences in heme dynamics between data recorded with either parallel polarization or magic angle is only expected within the first 200 fs.²⁵ Beyond 200 fs and within our time window of 50 ps, anisotropy signal is assumed to be quasi constant implying that data taken with parallel polarization and at magic angle have similar dynamics, thus allowing to compare this data set with previous measurements done at magic angle. After passing through the sample, the probe beam is focused onto the 80- μm input slit of the Triax 190 spectrometer, while using a 300 grooves/mm, 550-nm blaze wavelength grating, and focused onto a 1024 pixel CMOS array. Such a configuration allows for a probing window extending from 350 nm to 750 nm with a spectral resolution of 1.3 nm. Due to the small amount of sample, the oxidation state of the hemes as well as the possible degradation of the complexes is verified by recording the steady-state absorption of the protein complex using the probe beam directly. Note that by passing through the capillary, the probe beam contains an additional broad and featureless scattering signal that is, for the purpose of the study, assumed to be constant with wavelength and compensated by adjusting the amplitude scale

to zero above 720 nm as no pigment have significant absorbance beyond this wavelength.¹⁶

Data treatment. The subtraction between two set of raw transient data gives rise to the “double difference” data, as explained in the text and ESI, Figure S1, panel C. Since the probe pulses are temporally chirped by some hundreds of fs, the Group Velocity Dispersion (GVD) is corrected on the double difference data. In the case of the Chl a analysis, the raw transient data is first corrected for GVD then Chl a signal is extracted by subtracting a linear background from each delay time, as explained in ESI, Figure S3. In either case, the data are analyzed by globally fitting (GF) a selection of kinetics representative of the major transient spectral features. The resulting exponential components are then used as initial parameters to fit the Eigen-kinetics that results from a Singular Value Decomposition (SVD) of the whole data-set (while omitting the portion containing cross-phase modulation).²⁴ The number of exponential components as well as their values are then refined until they satisfactorily fit both the set of kinetics used in the GF and the Eigen-kinetics that result from the SVD. The corresponding Decay Associated Spectra (DAS) are generated for each data set. Concerning the analysis of the heme b , a frame-by-frame analysis complements the study by disentangling between the different processes. The frame-by-frame analysis consists in fitting the spectra at each time delay following a particular model, as described in ESI, Figure S10.

Results

While most studies on cytochromes focus on the intense Soret band region (~ 400 nm), this work uses the weaker α -band around 540–570 nm to monitor the hemes ultrafast dynamics. In the case of *cyt b_{6f}*, the Soret band region is spectrally congested²⁶ and the α -bands offer a clearer window, which permit to distinguish between the hemes with respect to the underlying Car and Chl a absorbance. Furthermore, it has been shown that the spectral features of the α -bands are highly sensitive to changes in the electronic states and coordination of the hemes.¹¹ With the excitation tuned at 515 nm, the hemes are excited via their β -bands while in their ferrous (reduced) state (see Figure 1). Due to specific environment, each heme has a particular redox potential: while the hemes b_p and b_n have a redox potential of -130 mV and -35 mV, respectively, the heme c_n and the heme f have a redox potential of +100 mV and +355 mV, respectively.²⁶ Consequently, it is possible to chemically control the reduction state of the hemes via ascorbate and dithionite. It is the control over the redox states that allows to spectrally distinguish the heme signals from the simultaneously excited Chl a and Car molecule.

The addition of ascorbate to the *cyt b_{6f}* preparation solely and fully reduces the heme f .⁸ After addition of stoichiometric excess of dithionite (1:10), the hemes b_p , b_n and c_n are all fully reduced within seconds.⁵ Since the hemes b_p and b_n are spectrally indistinguishable, both are analysed simultaneously and referred as the heme b .

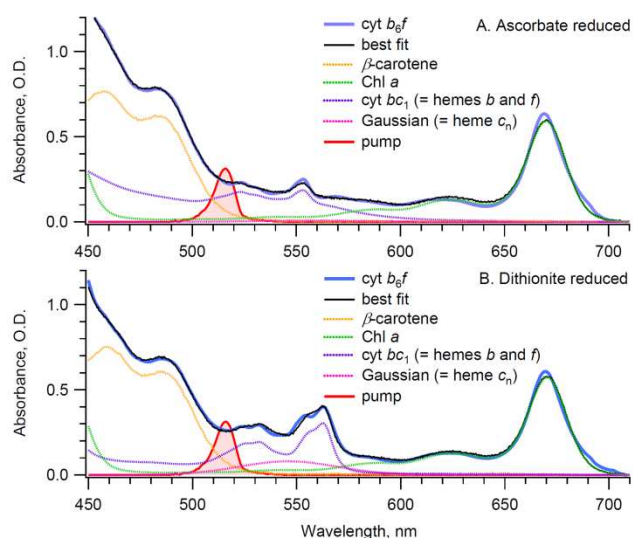


Figure 3: Modelling of the static absorbance of the *cyt b₆/f* complex (blue) after addition of (A) ascorbate and (B) dithionite, as in Figure 1. The *cyt b₆/f* spectrum is modeled by means of the Car (orange) and Chl *a* (green) absorbance; The *cyt bc₁* spectrum (purple) mimics that of the hemes *b* and *f*; The extra Gaussian (pink) represents the heme *c_n* spectrum. The Rieske protein is included in the *cyt bc₁* spectrum. Best fit is shown in black. The excitation pump spectrum is shown in red. Details of the fitting procedure are given in the ESI.

We consequently refer to both without distinction by omitting the subscript 'p' and 'n' in the rest of the manuscript, unless specified. The spectral characteristic of the ferrous hemes *b* and *c_n* is resolved by comparing the static spectra of the (ascorbate reduced) *cyt b₆/f* complex before and after addition of dithionite, as shown in Figure 1B (blue dashed curve). The resulting reduced-minus-oxidized absorbance spectrum of the ferrous (reduced) hemes *b* and *c_n* is then compared to that of the homologous *cyt bc₁* hemes *b* in Figure 2.¹¹ The reduced-minus-oxidized *cyt b₆/f* spectrum is more intricate than that of the homologous *cyt bc₁*, as expected due to the presence of the additional Car, Chl *a* and the heme *c_n*. The difference spectrum between the two cytochrome complexes is characterized by a broad band that maximizes at ~550 nm. Since Chl *a* has only minimal absorption in this region and since the Car *S₁*, that is expected to maximize at ~580 nm, is optically forbidden,²⁷ the broad positive absorbance band is solely attributed to the reduced-minus-oxidized heme *c_n*. This absorbance spectrum resembles the previously published heme *c_n* spectrum by Rappaport et al.,²⁶ and confirms that, in the presence of dithionite, the heme *c_n* is reduced and is absorbing part of the 515 nm excitation. In order to evaluate the relative absorbance of each of the pigments present in the sample, the *b₆/f* absorbance spectrum is fit by means of the monomeric Car, Chl *a*, *cyt bc₁* spectrum (to mimic that of the hemes *b* and *f*) and an extra Gaussian to reproduce the spectrum of the heme *c_n*, as depicted in Figure 3. The fit shows that all chromophores are initially excited, with Car absorbing more than one third of the excitation pulse. Consequently the transient data is expected to be dominated by the Car signal.

Table 1: Relative absorption of the excitation by the different pigments, as derived by the fitting of the static spectrum in Figure 3. Note that ascorbate only reduces the heme *f*, while dithionite fully reduces the *cyt b₆/f* complex. Calculations are shown in ESI.

	Car	Chl <i>a</i>	Heme <i>b</i> and <i>f</i>	Heme <i>c_n</i>
Ascorbate reduced	36%	6%	57%	1%
Dithionite reduced	38%	6%	44%	12%

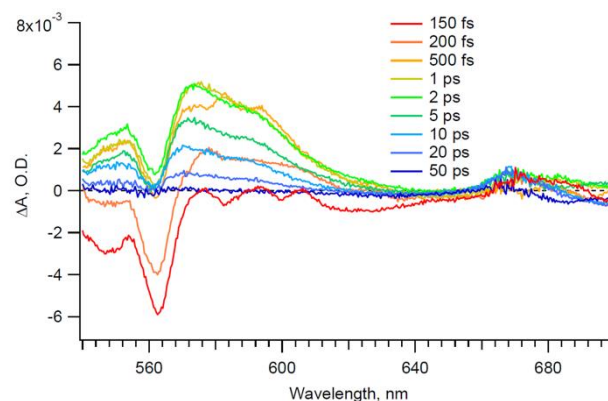


Figure 4: Spectra of the transient absorption signal from the *cyt b₆/f* complex after 515 nm excitation of the hemes *b* and *c_n* at selected time delays (Full range spectra are shown in the ESI).

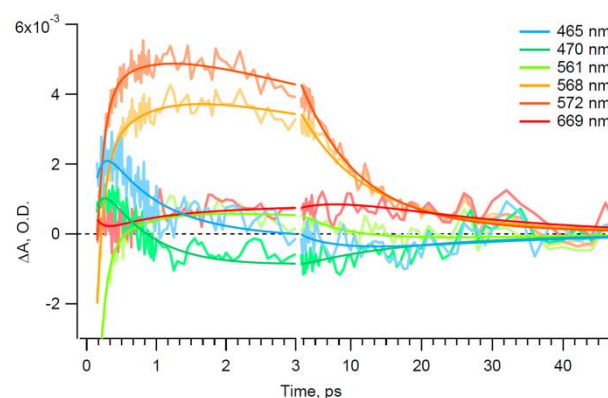


Figure 5: Kinetics of the Transient absorption signal of *cyt b₆/f* after 515 nm excitation of the hemes *b* and *c_n* and their best fit (smoothed lines) at selected wavelength. Note that the scale changes after 3 ps.

The transient signal resulting from the heme *b* and *c_n*, which is the focus of this paper, is isolated by subtracting the 2-dimensional time-wavelength transient data set corresponding to the complex, while the heme *f* is selectively reduced via ascorbate, from 2-dimensional time-wavelength transient data of the complex while all hemes are reduced via dithionite (see ESI, Figure S1 for details of the procedure). As described in Table 1, the relative absorption of the 515 nm light excitation by Chl *a* remains the same under both reducing conditions. On contrary, that of Car increases by about 5% (i.e. a change from 36% to 38% in overall absorbance corresponds to an increase of ~5% relative to the initial absorbance of Car). Consequently, the double difference data is expected to contain, on top of the transient signal from directly excited hemes *b* and *c_n*,

remaining signal from initially excited Car. Fortunately, the Car dynamics in this time-spectral window are well known²⁸ and easily distinguishable from the hemes signals. Spectra at selected time delays as well as kinetics at selected wavelength of the resulting double-difference data are shown in Figure 4 and Figure 5, respectively. The purpose of the double difference data is not to extract the sole signal contribution from the hemes *b* and *c_n*, but to substantially minimize the contribution from the initially excited Car and Chl *a*. The double difference data is indeed expected to contain some signal from both Car and Chl *a*, as the relative absorbance of Car varies slightly between the two sets of “simple” transient data and because the absorbance bands of Car and Chl *a* red-shift by about 1.8 and 0.4 nm, respectively, upon reduction of the cytochrome complex by dithionite (see ESI, Table S1). Spectral shifts of the pigments could in principle result in a comparable shift of their transient signal, thus affecting the double difference data. Nevertheless, in respect to the “simple” transient data, the double difference data improves the contrast between the hemes signals and the signal from Car and Chl *a* by a factor of ten.

Similar to the hemes *b* in the homologous cyt *bc₁*, while in their ferric states the hemes *b* are expected to be unresponsive under 515 nm excitation. Changes in the electronic state of the heme iron center are indeed not expected while exciting above 400 nm.²⁹ Accordingly, while the heme *b* is ferric (oxidized), the “simple” transient data (in opposition to the double difference data) does not show any signs of narrow band signal around 563 nm that would be representative of the heme’s photo-reduction (see Figure S1 A). Regarding the heme *c_n*, the fit in Figure 3 shows that while in its ferric (oxidized) state, the heme absorbance is negligible, absorbing only about 1% of the excitation pulse. We thus assume that the double difference data is devoid of any contribution from the ferric heme *c_n*. Concerning the heme *f*, its oxidation state is the same while performing both “simple” transient measurements and the lack of sharp features in the 550 nm region⁸ of the double difference data (Figure 4) proves that its signal contribution is effectively subtracted. The double difference data thus contains the well-defined signal from the ferrous heme *b* and *c_n*, superimposed with remaining typical signal from directly excited Car and Chl *a*.

At first sight, one can see in Figure 4 that part of the broad positive signal that extends from 540 nm to 600 nm and beyond corresponds to the expected Car *S₁* signal. On top of the latter signal sit sharp features in the 560 nm region that are associated with the heme *b* α -band as no other sharp absorbance band is present in this spectral region. The 670 nm region is marked by the Chl *a* *Q_y* signal that is rather weak with a lower signal-to-noise ratio. The data in this spectral region will thus be upheld by additional analysis.

In order to deconvolute the different processes involved in the double difference data, the kinetics in Figure 5 are globally fit. The fit results in a minimum of 4 exponential components. The whole surface data is then analyzed via SVD.

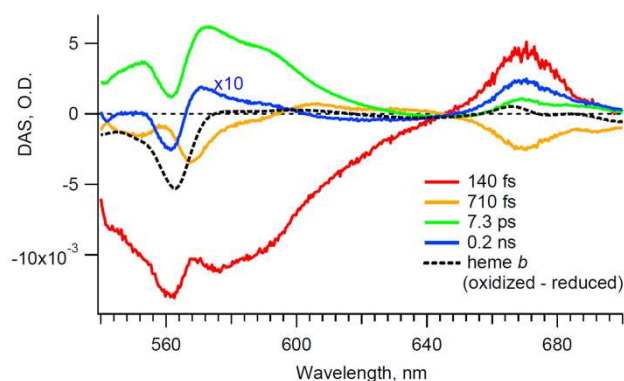


Figure 6: DAS of cyt *bc₁* complex after excitation of the hemes *b* and *c_n*. The oxidized-minus-reduced spectrum of the combined hemes *b* and *c_n* is superimposed for comparison only (black dashed curve).

The same four exponential decay components from the global fit are used to satisfactorily fit the Eigen-kinetics resulting from the SVD analysis (shown in ESI, Figure S5). Cross-checking the numbers of the fitting parameters and their values between the GF and the SVD analysis ensure that all major physico-chemical processes are captured and resolved. The resulting Decay Associated Spectrum (DAS) is shown in Figure 6.

We remind that in global analysis, the processes that have comparable lifetimes are usually merged and characterized by a single exponential component, which justify the small number of DAS components in Figure 6 although there are four different types of pigments contributing to the signals. Note that the 0.2 ns DAS component in Figure 6 is used to optimize the fitting results in the Chl *a* *Q_y* and Soret region. However due to its low amplitude and noise level of the data, it cannot be clearly resolved and can range from 50 ps up to few ns without significant alteration of the other three exponential decay components and corresponding DAS. This component is fixed to an arbitrary 0.2 ns to coincide with the expected relaxation time of the Chl *a* excited state¹⁵ that is either directly excited or indirectly via ultrafast energy transfer from Car.²⁸ This component seems to involve the hemes *b* as well, which suggests a possible coupling between Chl *a* and the hemes *b*, as discussed in the next section. The presence of the heme *b* signal in all DAS components indicates that the heme *b* undergoes gradual structural modifications rather than being described by specific states. However, global fitting methods are not able to render gradual changes. The indication for SVD analysis artifacts is the symmetry between spectral features within DAS whose exponential component are comparable. In the present case, both the 140 fs and 710 fs DAS have undulations in the 560 nm region that are opposite in sign and comparable in amplitude. Furthermore, that the α -band bleach in the 7.3 ps DAS is \sim 1 nm blue-shifted and has a larger (in amplitude) positive red-wing in respect to the oxidized-reduced spectrum (Figure 6). The SVD analysis therefore suggests that the bleach is superimposed with an electrochromic shift. In order to clearly resolve the spectral evolution of the heme *b*, we perform a complementary fit.

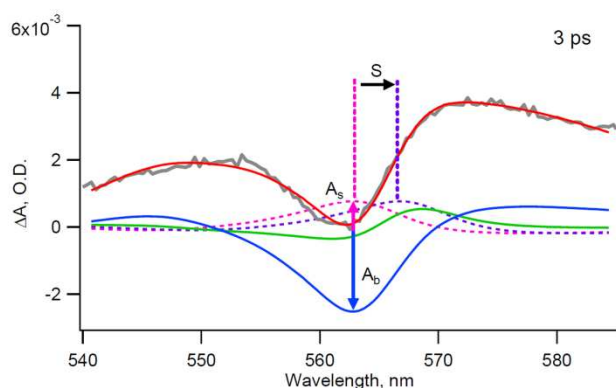


Figure 7: Fitting results at 3 ps. The fit (red curve) to the data (grey curve) consists of the oxidized-minus-reduced spectrum of heme *f* (blue curve) and the heme *f* band shift (green curve). The band shift itself is the difference between the fixed heme *f* reduced-minus-oxidized spectrum (pink dotted curves) and its shifted duplicate (purple dotted curves). The Gaussian used to model the background signal of the Car molecule is omitted for clarity.

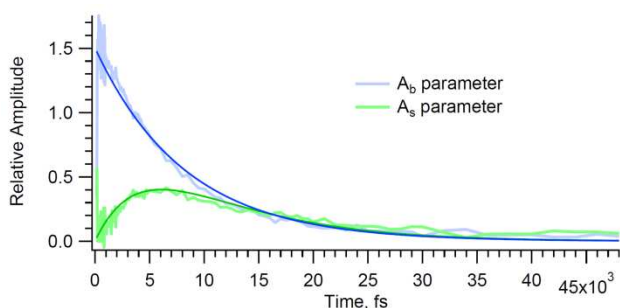


Figure 8: Time evolution of the principal fitting variables. See ESI, Figure S11 for the time evolution of all parameters.

From Figure 4, it is clear that part of the signal in the 560 nm region corresponds to the bleach of the heme *b*, while the SVD analysis suggests that the heme *b* concomitantly undergoes an electrochromic shift. Thus, for each time delay, the spectrum in the 560 nm region is fit as a bleach (by means of the heme *b* oxidized-minus-reduced spectrum difference) superimposed with a reconstructed shift of the heme *b* α -band. In this frame-by-frame analysis, the Car signal is compared to a Gaussian function that can be subtracted from the heme *b* signal. The amplitude, position and width of the Gaussian as well as the amplitude of the oxidized-minus-reduced heme *b* used to account for the bleach (A_b) and the amplitude of the oxidized-minus-reduced heme *b* spectrum used in modeling the shift (A_s) are all kept as free parameters. Only the magnitude of the shift (S) is fixed at specific values; the reason being that the parameters " A_s " and " S " are complementary for small shifts ($< \pm 10$ nm), i.e. an increase in " A_s " is compensated by the equivalent decrease in " S ". Hence the fitting procedure is repeated for multiple " S " values. Examples of the fit at various time delays are shown in Figure 7, while the parameter " S " is set to +4 nm (red shift). The evolution of the principal fitting variables is plotted in Figure 8. The " A_b " parameter represents the amplitude of the band responsible for the bleach, while the " A_s " parameter corresponds to the amplitude of the band responsible for the shift.

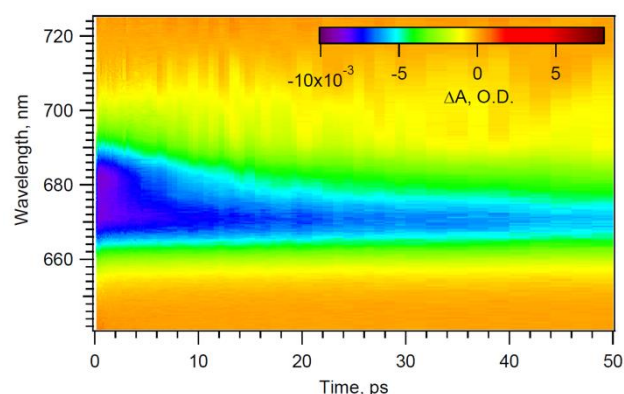


Figure 9: Chl *a* signal retrieved from the ascorbate (partially) reduced cyt *b₆/f* complex (heme *b* and *c* are oxidized).

Details of the fitting procedure and results are given in ESI. Irrespective of the choice of the " S " parameter, the " A_b " parameter decays mono-exponentially and the " A_s " parameter grows as a red-shift and reaches a maximum at 7 ps. The shift then relaxes concomitantly with the heme *b* bleach signal. The origin of the band-shift and its correlation with the bleach signal are discussed in the next section.

Regarding the Chl *a* signal, the DAS in the 670 nm region (Figure 6) shows bands that correspond precisely to the absorbance of the Chl *a* Q_y band. However the 140 and 710 fs DAS shows amplitudes that are twice larger than the ones actually monitored for Chl *a* (Figure 4). The Chl *a* signal analysis therefore needs to be confirmed. In order to refine the analysis, we extract the sole Chl *a* signal from the "simple" transient data (in opposition to the double difference data) as follow. In the 670 nm region, the Car signal is broad and featureless and modeled as a first degree polynomial (a line). The Chl *a* signal, shown in Figure 9, is extracted by subtracting the underlying Car signal at each time delay (see ESI for details of the fitting procedure, Figure S2). The deconvolution is done in the case in which the heme *b* and c_n are oxidized (Figure 9) and in the case when the complex is fully reduced via dithionite (not shown, but similar to Figure 9). While the hemes are fully oxidized as well as when they are fully reduced, two bands are distinguishable at 670 and 685 nm. The 670 nm band is assigned to the singlet state of cyt *b₆/f*-bound Chl *a*,¹⁷ and the 685 nm represents the enhanced (due to parallel polarization between pump and probe) stimulated emission (SE) of contaminant Chl *a*.¹⁷ The extracted Chl *a* signals is then analyzed independently in each data set by means of GF and SVD. Details of the SVD analysis can be found in ESI, Figure S6-S8. In each set, the same exponential components could fit both the kinetics (Figure 10) and the Eigen-kinetics resulting from the SVD analysis. As depicted by the DAS in Figure 11, only while the complex is fully reduced, a fourth exponential component was needed, resulting in an extra 670 nm band that appears and disappears in 90 and 650 fs, respectively. These extra dynamics coincide temporally and spectrally with the 140 fs and 710 fs DAS components shown in Figure 6.

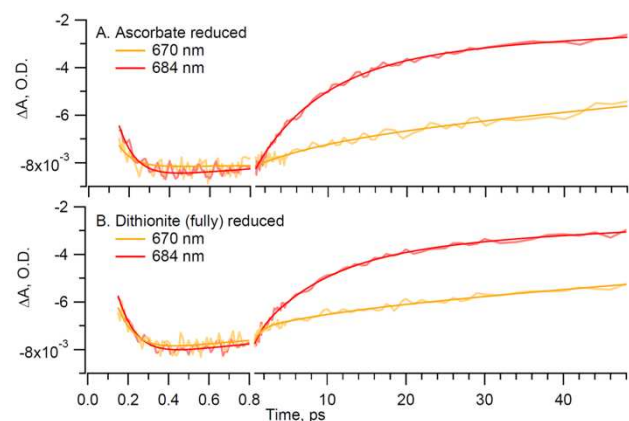


Figure 10: Kinetics of the retrieved Chl *a* signal from the cyt *b₆f* complex, while the complex is partially and fully reduced via ascorbate and dithionite, respectively. The smoothed lines are fits.

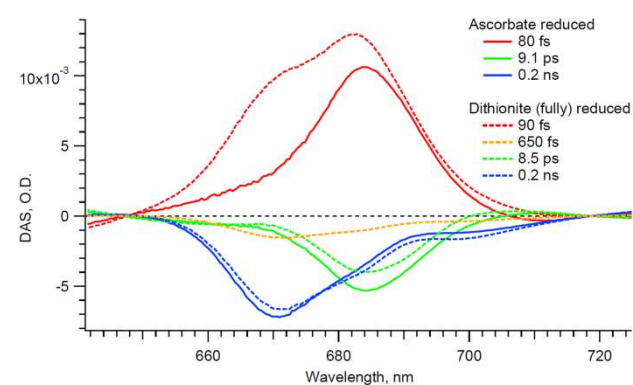


Figure 11: DAS of the different retrieved Chl *a* signals from the cyt *b₆f* complex while partially and fully reduced.

Note that a signal that decays in 90 fs still has 20 percent of its initial amplitude after 150 fs, which justify the resolution of the 90 fs DAS component even so the analyzed data set starts at 150 fs.

Discussion

Due to the distinct spectral features of the different chromophores, it is possible to analyze the data by zone of interest: (a) the heme *b* from 550 to 580 nm, (b) the Car molecule and (c) heme *c_n* from 540 to 640 nm, and (d) the Chl *a* *Q_y* band from 650 to 700 nm

(a) Signal from the hemes *b*. The broad signals, on which the sharp heme *b* features stand, are discussed as part of the Car and heme *c_n* signals analysis. In the light of the previous analysis of the homologous cyt *b₆c₁* complex, the heme *b* is thus expected to either dissipate the deposited energy via intra- or inter-molecular vibrations, to photo-dissociate from their axial ligand, to photo-oxidize, or to undergo an electrochromic shift as a response to rearrangement of its surrounding.¹¹ We evaluate each of the expected processes as follows:

Hemes *b* photo-dissociation and -oxidation. The heme *b* α -band bleach signal that is present in the 150 fs transient

spectra (Figure 4) indicates that the process is beyond our time resolution (<50 fs). The frame-by-frame analysis shows that this bleach signal decays mono-exponentially within picoseconds. We expect the bleach to be the signature of either photo-dissociation or photo-oxidation as it is the case in the homologous cyt *b₆c₁* complex.¹¹ Concerning photo-dissociation, in the cyt *b₆c₁* heme *c₁* as well as in cyt *c*, this process is characterized by a tri-exponential decay, i.e. a sub-picosecond, a 1-2 ps and a 6-7 ps relaxation,³⁰ which are all marked by strong excited state absorption (ESA, positive signal) spanning the 600 to 700 nm region.^{11, 31} The lack of such ESA signal as well as the absence of the 1-2 ps component indicates that the heme *b* does not undergo typical photo-dissociation from one of its axial ligand but most probably photo-oxidizes, as does the heme *b* in cyt *b₆c₁*.¹¹ In agreement with the DAS, the frame-by-frame analysis shows that the recovery of the heme *b*'s α -band bleach is taking place mono-exponentially in about 8.2 ps. Similarly to cyt *b₆c₁*, this signal is associated to the charge recombination between the heme and the ejected electron that is expected to reside in one of the surrounding aromatic amino acid, whose absorbance does not show in our spectral window. Even so the heme *b_n* is adjacent to the heme *c_n*, the latter is initially in its ferrous (reduced) state and is not expected to accept the photo-ejected electron from the heme *b*. Furthermore, the broad positive signal on which sits the heme *b*'s α -band signal in the 7.3 ps DAS component is better representative of the decay of the Car *S₁* state, as subsequently discussed, rather than that of the heme *c_n* spectrum. Thus the heme *c_n* is not expected to play the role of acceptor for the photo-ejected electron.

Hemes *b* vibrational relaxation and electrochromic shift. The frame-by-frame analysis clearly shows that the heme *b*'s α -band undergoes a red shift. While a blue shift usually refers, in heme-proteins, to the weakening of the guest–host interaction, the red shift is representative of an expansion of the heme macrocycle from a vibrationally excited ground state.³² Since a similar red-shift is also seen in free-based (devoid of metal center) single porphyrins,³³ we expect the extra energy to reside on the heme macrocycle, resulting in a nuclear reorganization of the heme,³⁴ which “stimulate some intra-molecular vibrational activity”.³² The picosecond rise of the red-shift suggests that the promotion to a vibrationally excited ground state is subsequent to the charge recombination, as in the case of the heme *f* within the same protein complex.⁸ The dynamics of the “*A_b*” (representing the bleach) and the “*A_s*” (representing the shift) parameters are thus respectively fit as a mono-exponential and a second sequential reaction as follow:

$$A_b(t) = A_{b_0} \cdot e^{-k_{cr}t} \quad (1)$$

$$A_s(t) = A_{b_0} \cdot \frac{k_{cr}}{(k_{cr} - k_{relax})} \cdot (e^{-k_{cr}t} - e^{-k_{relax}t}) \quad (2)$$

where “*A_{b0}*” is the initial bleach amplitude; “*k_{cr}*” and “*k_{relax}*” correspond to the rate of charge recombination and rate of heme structural relaxation, respectively. Based on this model,

best fit is found when “S” (the shift magnitude) is about 4.0 nm, with charge recombination rate, “ k_{cr} ”, and the relaxation rate of the residual vibrational energy, “ k_{relax} ”, are equal to $(8.2 \text{ ps})^{-1}$ and $(4.6 \text{ ps})^{-1}$, respectively.

The small discrepancy between the fit and the data in the 550–560 nm region (Figure 7) is in fact recurrent in multiple time delays (see ESI, Figure S15) and could be accounted for by a slight broadening of the band. However, due to the actually large number of fitting parameters and the noise level of the data, we do not speculate further.

(b) Signal from β -carotene. In the spectral region from 540 to 640 nm, the transient signal is dominated by a broad band superimposed with sharp undulations around 565 nm. While the sharp undulations are solely assigned to the heme b activity, the broad feature can either be attributed to the heme c_n signal that is expected to peak around 550 nm²⁶ or to the Car S_1 signal that maximizes at ~ 580 nm.³⁵ The broad negative signal in the 140 fs DAS, the bimodal feature with the zero crossing point at 690 nm in the 710 fs DAS as well as the broad positive signal in the 7.3 ps DAS are all typical, in spectral features and dynamics, of the Car excited state relaxation mechanisms:³⁵ Internal conversion from S_2 to the hot S_1 state in 140 fs, followed by a 710 fs intramolecular vibrational relaxation to the lowest S_1 state and subsequent ground state recovery in 7.3 ps. It is important to mention that since multiple processes are taking place in the same spectral window with comparable lifetimes, the exponential components can only be taken as approximations. For example, the decay of the Car S_1 , which is about 9 ps when analyzed separately,³⁵ is now associated with the ground state recovery of the heme b α -band bleach in the 7.3 ps DAS. As previously mentioned, residual transient signal from Car in the double difference data is expected to be $\sim 5\%$ of the absolute Car signal, which is about 40 mO.D. at 580 nm after 1 ps (see Figure S2). The remaining Car signal in the double difference data is consequently expected to be about 2 mO.D. at 580 nm after 1 ps, while it is actually ~ 4 mO.D. (Figure 4). This extra short-lived signal is discussed as originating from the heme c_n . Regarding the origin of the Car signal, Car molecules could either be directly excited or indirectly via pulse-limited energy transfer from one of the excited hemes. The short distance between the Car molecule and the hemes b_n and c_n (Figure 12)⁶ is actually ideal for ultrafast energy transfers. However the yield of energy transfer also depends on the overlap between the hemes fluorescence and the Car absorbance. The fluorescence of embedded cyt is expected to be minimal in the region below 550 nm³⁶ with minor overlap with the Car absorption spectrum. Hence the probability of energy transfer from the hemes to Car is assumed to be negligible. The Car signal is thus assumed to originate solely from directly excited Car molecules.

(c) Signal from the heme c_n . The broad negative signal in the 140 fs DAS component (Figure 6) is about twice as large in amplitude as expected if it would solely represent the Car S_2 to Car S_1 internal conversion.^{27, 35} Part of this broad negative

signal in the 140 fs DAS component can be attributed to the recovery of an initially bleached heme c_n . Indeed, the broad underlying negative signal present in the 150 fs transient spectra (Figure 4) indicates the presence of an initially excited pool of heme c_n . While usual photo-oxidation and photo-dissociation recovery involve vibrational and conformational relaxation that takes place within picoseconds,¹² this 140 fs recovery suggests a purely electronic relaxation similar to the one monitored in cyt c .³⁷

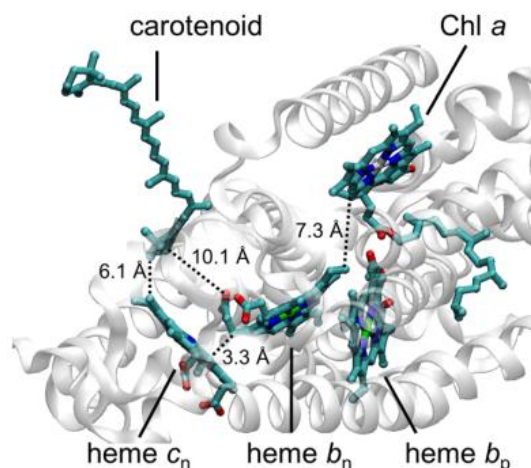


Figure 12: Prosthetic groups of the cytochrome b_6f complex and their edge-to-edge distances. Crystallographic data from the pdb file 2e74.⁶

(d) Signal from Chl a . As previously mentioned, the 670 nm signal, corresponding to the Chl a Q_y absorbance band, can originate from directly excited Chl a . The 670 nm signal could as well be the result of indirect excitation, via the initially excited Car, since ultrafast (unresolved, sub ~ 50 fs) energy transfer from Car to Chl a is expected.²⁸ Unfortunately, we do not differentiate between the two processes. The 670 nm band that appears in 90 fs and decays in 650 fs implies that an interaction is taking place between cyt b_6f -bound Chl a and the reduced hemes b and/or c_n . Concerning the nature of the Chl a signal, it cannot correspond to typical Chl a relaxation as we would monitor similar dynamics while the cyt complex is only partially reduced with ascorbate. Such signal have not been resolved in previous excited state investigation of the ferric cyt b_6f embedded Chl a .^{15, 17} The fact that the 90 fs bleach and 650 fs recovery of the Chl a have not previously been resolved in transient nor in fluorescent measurements of directly excited Chl a ¹⁵ nor indirectly via excitation of Car²⁸ implies that this ultrafast process is solely a results of the heme's excitation. Additionally, the bleaching of Chl a implies a drastic reorganisation of its electronic configuration. Or, it is well-known that Chl a molecules are able to incorporate extra electron onto their porphyrin ring and are commonly used as an intermediate for intra-molecular electron transfer.^{38, 39} Furthermore, it has been suggested by Savikhin et al.¹⁷ that, within the cyt b_6f , the excited Chl a relaxes by electron-exchange mechanism with a near-by aromatic amino-acid, implying the formation of a Chl a anion. It is therefore

reasonable to suggest that the signal monitored corresponds to the formation and decay of a Chl *a* anion species in 90 and 650 fs, respectively. The nature of the conjugated electron donor/acceptor is however unclear as none of the hemes shows clear signs of photo-induced oxidation/reduction in these two time scales. The edge to edge distances from the heme b_n , b_p and c_n to the Chl *a* are about 6, 13 and 20 Å,⁶ respectively, as shown in Figure 12. Due to the ultrafast nature of the process and the high distance dependence of electron and energy transfer, it is the adjacent heme b_n that is expected to interact with the Chl *a*. Thus, we intuitively suspect the b -heme that undergoes photo-oxidation to play the role of initial electron donor and final acceptor, along with possible amino-acids intermediaries. While the nature of the interaction between the hemes and the Chl *a* is still under investigation, this work represents the first evidence that, contrary to previous assumptions,⁴⁰ Chl *a* has functions beside being simple evolutionary relic used for structural purposes only: it is directly implicated in the heme's photochemistry.

Conclusions

After excitation of the cyt b_{6f} complex at 515 nm, the relaxation dynamics of the hemes b and c_n are retrieved by means of ultrafast broad-band transient absorption. Besides the typical Car and Chl *a* ground state recovery, the analysis shows evidence for at least three mechanisms of heme relaxation:

- (1) Part of the ferrous b hemes undergo pulse limited photo-oxidation, alike in the homologue bc_1 . The liberated electron is assumed to reside in one of the adjacent amino-acid. The following charge recombination takes place in about 8.2 ps. The Cyt b_{6f} thus represents an ideal organic model for the study of charge separation, as the chromophores are few and well separated spectroscopically.
- (2) Subsequent to the charge recombination, the b hemes red-shift by ~4.0 nm, which is indicative of a vibrationally excited ground state. Modeling of the shift dynamics shows that this excited state relaxes in about 4.6 ps.
- (3) The ferrous heme c_n undergoes an ultrafast relaxation in 140 fs. Given the ultrafast nature of the process, the relaxation is suggested to be primarily electronic. Minor conformational relaxations are however not excluded.

Additionally, The Chl *a* expresses a bleach signal that appears and decays in 90 and 650 fs, respectively, corresponding most probably to a Chl *a* anion species. Because this signal is only present when the complex is fully reduced, it unambiguously indicates that the Chl *a* molecule have functions besides being simple evolutionary relics: it participates in the deactivation processes of the photo-excited hemes. The nature of the interaction is however unclear.

While this study resolves some of the fundamental ultrafast relaxation dynamics of the hemes b and c_n , it also calls for

further investigations. In particular, the ultrafast formation of the Chl *a* anion can be confirmed by ultrafast infrared analysis, and the possible implication of surrounding amino acids as electron donor/acceptor can be verified by means of ultrafast spectroscopy in the ultraviolet region. These investigations are underway.

ACKNOWLEDGMENT

The authors warmly thank Professor Majed Chergui, André al Haddad and Frank van Mourik from EPFL, Lausanne-CH, for their effective technical support; as well as Professor William A. Cramer from Purdue University, West Lafayette-USA, for providing with the precious sample. Thanks also to Professor Julia Weinstein, from the University of Sheffield, for fruitful discussions. This research was supported by the NCCR MUST, funded by the Swiss National Science Foundation, via the FP7 Marie Curie COFUND (AAPC), and by the US NIHGM5-038323 to W. A. Cramer (RA).

ABBREVIATIONS

Car, β -carotene; Chl *a*, Chlorophyll *a*; CN-PAGE, clear native polyacrylamide gel electrophoresis; CR, charge recombination; Cyt, cytochrome; DAS, Decay Associated Spectrum; ESA, Excited State Absorption; FeCN, ferricyanide; n, p, electrochemically negative and positive side of the membrane; SVD, Singular Value Decomposition; SE, stimulated emission; UDM, undecyl maltoside.

Notes and references

1. W. A. Cramer, H. Zhang, J. Yan, G. Kurisu and J. L. Smith, *Annu. Rev. Biochem.*, 2006, **75**, 769-790.
2. D. Xia, L. Esser, M. Elberry, F. Zhou, L. Yu and C.-A. Yu, *J. Bioenerg. Biomembr.*, 2008, **40**, 485-492.
3. C. Lange and C. Hunte, *Proc. Nat. Acad. Sci. USA*, 2002, **99**, 2800-2805.
4. W. A. Cramer, H. Zhang, J. Yan, G. Kurisu and J. L. Smith, *Biochemistry*, 2004, **43**.
5. A. A. P. Chauvet, R. Agarwal and W. A. Cramer, *Rev. Sci. Instrum.*, 2015, **86**.
6. E. Yamashita, H. Zhang and W. A. Cramer, *J. Mol. Biol.*, 2007, **370**, 39-52.
7. A. Chauvet, T. Tibiletti, S. Caffarri and M. Chergui, *Rev. Sci. Instrum.*, 2014, **85**.
8. A. A. P. Chauvet, R. Agarwal, A. al Haddad, F. van Mourik and W. A. Cramer, *Phys. Chem. Chem. Phys.*, 2016, **18**, 12983-12991.
9. C. Consani, G. Auböck, O. Bräm, F. van Mourik and M. Chergui, *J. Chem. Phys.*, 2014, **140**, 025103.
10. M. Chergui, in *Comprehensive Biophysics*, ed. E. H. Egelman, Oxford: Academic Press, 2012, vol. 1, pp. 398-424.
11. A. A. P. Chauvet, A. Al Haddad, W.-C. Kao, F. Van Mourik, C. Hunte and M. Chergui, *Phys. Chem. Chem. Phys.*, 2014, **17**, 2143-2151.

12. M. H. Vos, A. Battistoni, C. Lechauve, M. C. Marden, L. Kiger, A. Desbois, E. Pilet, E. de Rosny and U. Liebl, *Biochemistry*, 2008, **47**, 5718-5723.
13. T. Mirkovic, E. E. Ostroumov, J. M. Anna, R. van Grondelle, Govindjee and G. D. Scholes, *Chem. Rev.*, 2016.
14. T. Kallas, in *Photosynthesis: Advances in Photosynthesis and Respiration*, 2012, vol. 34, pp. 501-560.
15. E. J. G. Peterman, S.-O. Wenk, T. Pullerits, L.-O. Pålsson, R. van Grondelle, J. P. Dekker, M. Rögner and H. van Amerongen, *Biophys. J.*, 1998, **75**, 389-398.
16. M. Sang, F. Ma, J. Xie, X.-B. Chen, K.-B. Wang, X.-C. Qin, W.-D. Wang, J.-Q. Zhao, L.-B. Li, J.-P. Zhang and T.-Y. Kuang, *Biophys. Chem.*, 2010, **146**, 7-12.
17. N. Dashdorj, H. Zhang, H. Kim, J. Yan, W. A. Cramer and S. Savikhin, *Biophys. J.*, 2005, **88**, 4178-4187.
18. H. Kim, N. Dashdorj, H. Zhang, J. Yan, W. A. Cramer and S. Savikhin, *Biophys. J.*, 2005, **89**, L28-L30.
19. S. S. Hasan and W. A. Cramer, *Phil. Trans. R. Soc. B*, 2012, **367**, 3406-3411.
20. S. S. Hasan, E. A. Proctor, E. Yamashita, N. V. Dokholyan and W. A. Cramer, *Biophys. J.*, 2014, **107**, 1620-1628.
21. D. Baniulis, H. Zhang, E. Yamashita, T. Zakharova, S. S. Hasan and W. A. Cramer, in *Photosynthesis Research Protocols, Methods in Molecular Biology*, ed. R. Carpentier, Humana Press Inc, Totowa, NJ, 2011, vol. 684, pp. 65-77.
22. H. Zhang, J. P. Whitelegge and W. A. Cramer, *J. Biol. Chem.*, 2001, **276**, 38159-38165.
23. A. Lisibach, E. Casartelli and N. Schmid, ASME 2010 3rd Joint US-European Fluids Engineering Summer Meeting and 8th International Conference on Nanochannels, Microchannels, and Minichannels, Montreal, Quebec, Canada, 2010.
24. J. Helbing, L. Bonacina, R. Pietri, J. Bredenbeck, P. Hamm, F. van Mourik, F. Chaussard, A. Gonzalez-Gonzalez, M. Chergui, C. Ramos-Alvarez, C. Ruiz and J. López-Garriga, *Biophys. J.*, 2004, **87**, 1881-1891.
25. C.-K. Min, T. Joo, M.-C. Yoon, C. M. Kim, Y. N. Hwang, D. Kim, N. Aratani, N. Yoshida and A. Osuka, *J. Chem. Phys.*, 2001, **114**, 6750-6758.
26. J. Alric, Y. Pierre, P. Picot, J. Lavergne and F. Rappaport, *Proc. Nat. Acad. Sci. USA*, 2005, **102**, 15860-15865.
27. J. L. Pérez Lustres, A. L. Dobryakov, A. R. Holzwarth and M. Veiga, *Angew. Chem.*, 2007, **46**, 3758-3761.
28. P. Zuo, B.-X. Li, X.-H. Zhao, Y.-S. Wu, Ai, X.-C., J.-P. Zhang, L.-B. Li and T.-Y. Kuang, *Biophys. J.*, 2006, **90**, 4145-4154.
29. Y. Gu, P. Li, J. T. Sage and P. M. Champion, *J. Am. Chem. Soc.*, 1993, **115**, 4993-5004.
30. C. Consani, O. Bräm, F. van Mourik, A. Cannizzo and M. Chergui, *Chem. Phys.*, 2012, **396**, 108-115.
31. W. Wang, X. Ye, A. A. Demidov, F. Rosca, T. Sjodin, W. X. Cao, M. Sheeran and P. M. Champion, *J. Phys. Chem. B*, 2000, **104**, 10789-10801.
32. J. Rodriguez, C. Kirmaier and D. Holten, *J. Phys. Chem.*, 1991, **94**, 6020-6029.
33. J. Rodriguez, C. Kirmaier, M. R. Johnson, R. A. Friesner, D. Holten and J. L. Sessler, *J. Am. Chem. Soc.*, 1991, **113**, 1652-1659.
34. T. G. Spiro, J. D. Stong and P. Stein, *J. Am. Chem. Soc.*, 1979, **101**, 2648-2655.
35. T. Lenzer, F. Ehlers, M. Scholz, R. Oswald and K. Oum, *Phys. Chem. Chem. Phys.*, 2010, **12**, 8832-8839.
36. O. Bräm, C. Consani, A. Cannizzo and M. Chergui, *J. Phys. Chem. B*, 2011, **115**, 13723-13730.
37. V. Karunakaran, *Chem. Phys. Chem.*, 2015, **16**, 3974-3983.
38. A. Chauvet, N. Dashdorj, J. H. Golbeck, T. W. Johnson and S. Savikhin, *J. Phys. Chem. B*, 2012, **116**, 3380-3386.
39. A. Chauvet, J. Sarrou, S. Lin, S. P. Romberger, J. H. Golbeck, S. Savikhin and K. E. Redding, *Photosynth. Res.*, 2013, **116**, 1-9.
40. Pierre, Y., C. Breyton, Y. Lemoine, B. Robert, C. Vernotte and J.-L. Popot, *J. Biol. Chem.*, 1997, **272**, 21901-21908.